Available online at www.sciencedirect.com
ScienceDirect
International Journal of Pharmaceutics 355 (2008) 195–202
INTERNATIONAL JOURNAL OF PHARMACEUTICS
www.elsevier.com/locate/ijpharm

Physical characterization of oleanolic acid nonsolvate and solvates prepared by solvent recrystallization

Henry H.Y. Tong [a], H.B. Wu [b], Y. Zheng [c], J. Xi [c], Albert H.L. Chow [d], Chak K. Chan [b,*]

[a] *School of Health Sciences, Macao Polytechnic Institute, Macao, China*
[b] *Department of Chemical Engineering, Hong Kong University of Science and Technology, Clear Water Bay, Kowloon, Hong Kong, China*
[c] *Institute of Chinese Medical Sciences, University of Macau, Macao, China*
[d] *School of Pharmacy, The Chinese University of Hong Kong, Hong Kong, China*

Received 28 August 2007; received in revised form 3 December 2007; accepted 6 December 2007
Available online 15 December 2007

Abstract

Oleanolic acid is a naturally occurring compound used clinically in China for the treatment of hepatitis B. The solid-state chemistry of oleanolic acid recrystallized from a variety of solvents was investigated. Glassy materials were prepared from dichloromethane and chloroform solvents. The oleanolic acid non-solvate prepared from acetone (OA-acetone), and the two oleanolic acid solvates prepared from methanol (OA-methanol) and ethanol (OA-ethanol) were physicochemically characterized. Upon desolvation, both the methanol and ethanol solvates were found to undergo phase transformation to a crystalline phase similar to OA-acetone around 190–195 °C. The PXRD patterns of commercial pharmaceutical grade OA and the OA-methanol were similar, so the commercial form is probably desolvated oleanolic acid methanol solvate.

Keywords: Oleanolic acid; Solvates; Solvent recrystallization; Solid-state transition

1. Introduction

Oleanolic acid (OA), a naturally occurring pentacyclic triterpenoid (Fig. 1a), is a biologically active marker compound commonly present in Chinese herbs such as *Akebia trifoliata* (in Chinese, *mu tong*) and listed in the 2005 China Pharmacopoeia. Pharmacological studies of OA have reported that it offers hepatoprotection against chemically-induced liver injury (Liu, 2005). The underlying mechanisms are possibly related to anti-oxidant activity, anti-inflammatory action, and its induction of metallothionein, a small cysteine-rich protein acting like glutathione in the body's defense against toxic insults (Liu, 2005). In addition, it has been recently demonstrated that OA's hepatoprotective action works at least in part through inhibiting the liver's mitochondrial permeability transition (Tang et al., 2005). OA in tablet form is available in China over the counter as a health supplement. Clinically, it has been used in the treatment of hepatitis, and as an adjunct therapy to prevent hepatotoxicity induced by anti-tuberculous medications such as isoniazid and pyrazinamide (Wang, 2003; Chen et al., 2005).

Being hydrophobic (Fig. 1a), OA exhibits solubility problems. Pharmaceutical grade OA does not dissolve to a detectable level (<1 μg/ml by HPLC) in buffer solutions (at pH 1 or 7) after 120 min at 37 °C (unpublished data). Due to poor absorption and extensive metabolic clearance, OA has an absolute bioavailability in rats of only 0.7% at oral doses of 25 and 50 mg/kg (Jeong et al., 2007). In a human pharmacokinetic study of OA capsules, T_{max} was reported to be 5.2 h, indicating that OA is not released immediately (Song et al., 2006). The potential therapeutic benefits of OA are widely known, but there has not been any detailed investigation of the solid-state properties which may account for its poor aqueous solubility and oral absorption. The present study aimed to prepare different crystalline forms of OA by solvent recrystallization and to characterize them using established solid-state techniques. The objective was to gain a better understanding of the solid-state behavior of OA which might enable the development of a more consistent and efficacious OA oral formulation.

* Corresponding author. Tel.: +852 2358 7124; fax: +852 2358 0054.
E-mail address: keckchan@ust.hk (C.K. Chan).

0378-5173/$ – see front matter © 2007 Elsevier B.V. All rights reserved.
doi:10.1016/j.ijpharm.2007.12.005

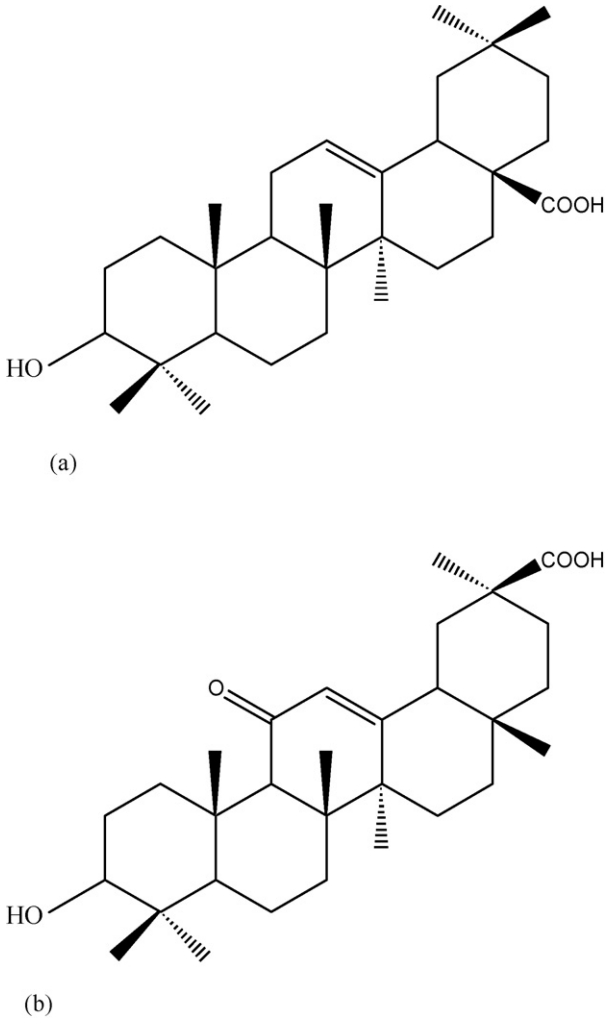

Fig. 1. Chemical structure of (a) oleanolic acid; (b) glycyrrhetinic acid.

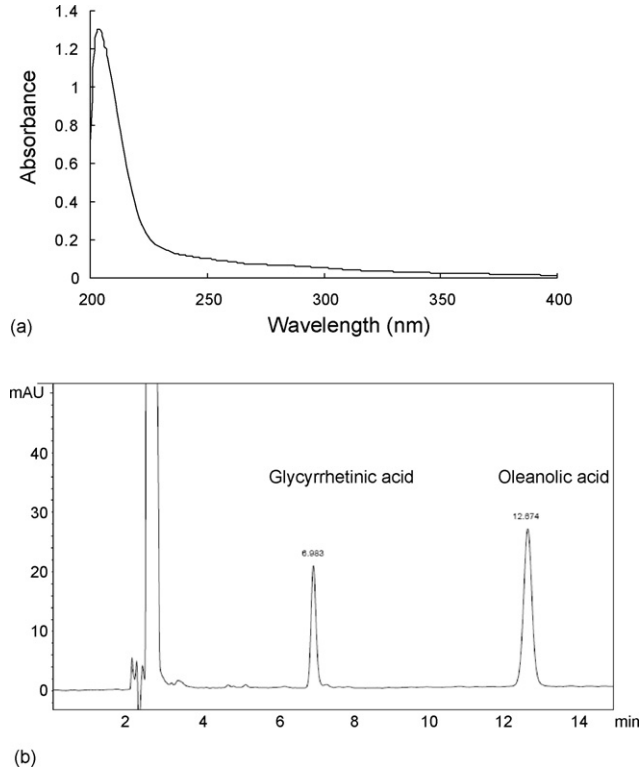

Fig. 2. (a) UV spectrum of oleanolic acid in absolute ethanol; (b) HPLC chromatogram in oleanolic acid assay.

2. Materials and methods

2.1. Materials

Pharmaceutical grade OA raw material (OA–RW) (purity ≥ 95%) was purchased from International Laboratory, San Bruno, USA. Standard OA (minimum purity 97%) was purchased from Sigma, USA, and a glycyrrhetinic acid standard was obtained from the China's National Institute for the Control of Pharmaceutical and Biological Products. The standards were used without further purification. All the methanol, absolute ethanol, dichloromethane, chloroform, acetonitrile and acetone used were of either analytical or HPLC grade. Sodium dodecyl sulphate was purchased from USB Corporation, USA. All the water used was double distilled.

2.2. Preparation of OA through solvent recrystallization

OA samples were prepared using cold crystallization or solvent evaporation methods. In the cold crystallization method, OA–RW powder was dissolved in an appropriate organic solvent at a temperature close to the boiling point of the solvent, and the solution was then cooled within a few hours down to 4 °C. In the solvent evaporation method, OA–RW was dissolved in an appropriate organic solvent at room temperature, and the solution was then allowed to evaporate at room temperature in a dark place for several weeks until visual examination showed that it was dry. In both methods, the OA was then harvested by filtration and dried on the filter paper with minimal trituration.

2.3. UV and HPLC characterization of oleanolic acid

The UV spectrum of oleanolic acid in absolute ethanol at 60 μg/ml was recorded using a DU-640 UV/vis spectrometer from Beckman Coulter, USA (Fig. 2a).The HPLC analysis of the oleanolic acid followed the protocol reported by Chen et al. (2003), with slight modifications. The analysis employed an Agilent 1100 series HPLC system, a 250 mm × 4.6 mm Agilent 5 μm Zorbax SB-C18 column, and a photodiode array detector (DAD) scanning the 190–400 nm range. Injection volume was 20 μl. The mobile phase was composed of acetonitrile and 0.5% phosphoric acid (85:15). It was eluted isocratically at a flow rate of 1.0 ml min^{-1}. The wavelength chosen for oleanolic acid quantification was 204 nm. Glycyrrhetinic acid, with a chemical structure similar to oleanolic acid (Fig. 1b), was used as an internal standard at 15–32 μg/ml. The glycyrrhetinic acid and oleanolic acid eluted as two distinct peaks with retention times of 6.9 min and 12.7 min, respectively (Fig. 2b). A calibration curve based on the AUC ratio between oleanolic acid and glycyrrhetinic acid had excellent linearity ($R^2 > 0.9994$). The

detection limit for oleanolic acid using this HPLC protocol was 1 μg/ml.

2.4. GC analysis of oleanolic acid solvates

The methanol and ethanol content of the OA samples were measured using gas chromatography (Model 5890, Series II, Hewlett Packard, USA). The gases were sampled with a Hewlett Packard headspace sampler (Hewlett Packard). The injection volume was 10 μl, The oven, injector and detector temperatures were maintained at 120, 250 and 280 °C, respectively. The carrier gas was helium at a flow rate of 1 μl/min. The methanol and ethanol target peaks were calibrated in the range of 0.5–20 μl. Excellent linearity was observed (methanol: $R^2 > 0.9998$; ethanol: $R^2 > 0.9999$). The samples were heated to 150 °C and equilibrated for 30 min before injection. All measurements were in triplicate from three independent samples.

2.5. Powder X-ray diffractometry (PXRD) and variable-temperature powder X-ray diffractometry (VT-PXRD)

The oleanolic acid samples were packed into sample holders. All the samples studied were fine enough to allow direct PXRD without the need for trituration. The PXRD patterns were recorded with a Philips powder X-ray diffraction system, Model PW 1830, using a 3 kW Cu anode ($\lambda = 1.540562$ Å) over a 2θ interval of 5.0–30.0°. The step size was 0.05°, with a counting time of 2 s. VT-PXRD patterns were recorded using a Panalytical, X'pert Pro diffractometer with an ultra-fast X-ray detector (Model: X'celerator). The measurements were carried out with Cu Kα radiation ($\lambda = 1.540562$ Å) at 40 kV and 40 mA. The scanning was conducted in continuous mode over a 2θ range from 5.0° to 30.0° in increments of 0.033°. Once a vacuum had been established inside the sample chamber, VT-PXRD patterns were obtained at every 15 °C increment from 30 to 180 °C.

2.6. Thermal analysis

Thermogravimetric (TGA) analysis was performed in an open pan using a PerkinElmer TGA 7 thermogravimetric analyzer with a TAC7/DX thermal analysis controller. Approximately 10 mg of the material (accurately weighed) was scanned at 10 °C min^{-1} from 50 to 400 °C.

Differential scanning calorimetry (DSC) was performed using a PerkinElmer Pyris 1 differential scanning calorimeter (with Pyris Manager software). Indium ($T_m = 156.6$ °C; $\Delta H_f = 28.45$ J g^{-1}) was used for calibration. Accurately weighed samples (1.5–2.0 mg) were placed in hermetically sealed aluminum pans with pinholes and scanned at 10 °C min^{-1} under nitrogen purge.

2.7. Variable temperature Fourier-transform infrared (VT-FTIR) spectroscopy

Reflectance spectra from powdered samples were recorded using a PerkinElmer Spectrum BX Fourier transform infrared spectrometer (PerkinElmer, Beaconsfield, Buckinghamshire, UK) with a self-fabricated temperature controlled sample holder which was able to maintain temperatures between room temperature and 90 °C with a precision of ±0.5 °C. Sixteen scans were performed on each sample. The resolution was 4 cm^{-1}. After equilibrating to 25 °C over 10 min, the samples were scanned from 4000 to 400 cm^{-1} in intervals of 2 cm^{-1}. The temperature was then increased at 10 K min^{-1} to 90 °C, and the samples were scanned again with the same conditions after equilibrating to 90 °C over 10 min.

2.8. Powder dissolution

8.5 ± 0.2 mg of the recrystallized oleanolic acid was added to 200 ml of water containing 1% (w/v) sodium lauryl sulphate in an amber glass bottle in a D-91126 shaking water bath (Schwahach FRG, Germany) protected from light. The temperature was controlled at 37.0 ± 0.5 °C, and the agitation speed was set at 100 rpm. At appropriate time intervals, 2 ml samples were withdrawn, filtered with a 0.22 μm membrane filter, and assayed using HPLC. The samples were also subjected to PXRD to monitor any potential phase transformation. All data points were triplicated.

2.9. Specific surface area

Specific surface area was determined by BET nitrogen adsorption using an Autosorb-1 Series surface area analyzer (Quantachrome, USA). The samples were placed in glass sample holders and outgassed with helium at 40 °C for 12 h before analysis. Nitrogen was used as the adsorbate, and 11 BET points were recorded as the specific surface area of the sample. PXRD measurements confirmed that no phase transformation occurred during the specific surface area determination.

2.10. Scanning electron microscopy

The morphology of the oleanolic acid samples was characterized using scanning electron microscopy (Model: JSM 6300F, JEOL, Japan) at 15,000× magnification.

3. Results and discussion

A transparent glassy material was obtained with either dichloromethane or chloroform as the solvent in both cold crystallization and solvent evaporation. Needle-shaped crystals were obtained when methanol, ethanol, acetone or acetonitrile was the solvent. SEM examination revealed that the OA–RW was in the form of fine, prismatic crystals, while the OA recrystallized from methanol, ethanol or acetone had fine needle-shaped crystals (Fig. 3A–D). This corresponds to the description of oleanolic acid in the Merck Index, which states that fine needles can be obtained from alcoholic solutions (Neil et al., 2001). The PXRD patterns of OA samples crystallized by fast cooling from chloroform or dichloromethane exhibited distinct "halo" patterns, indicating an amorphous nature (Fig. 4). In Fig. 4, three crystalline forms can be identified, corresponding to OA–RW

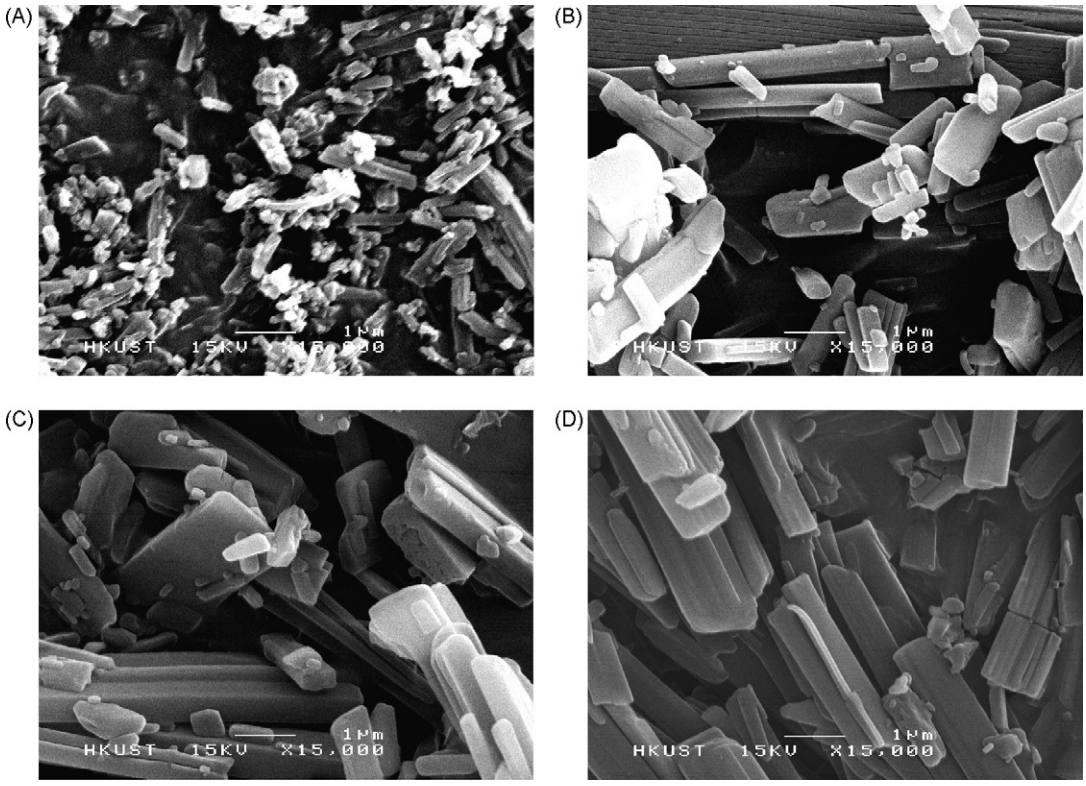

Fig. 3. SEM photographs of oleanolic acid samples: raw material (A), methanol solvate (B), ethanol solvate (C), and non-solvate (D).

and OA recrystallized from methanol, OA recrystallized from ethanol, and OA recrystallized from acetone or acetonitrile. Similar PXRD patterns were observed in OA samples recrystallized by slow evaporation from various organic solvents (data not shown). To the best of our knowledge, the solid-state characteristics of oleanolic acid have not previously been reported.

The OA–RW and the three newly discovered crystalline materials prepared by cold crystallization from methanol, ethanol

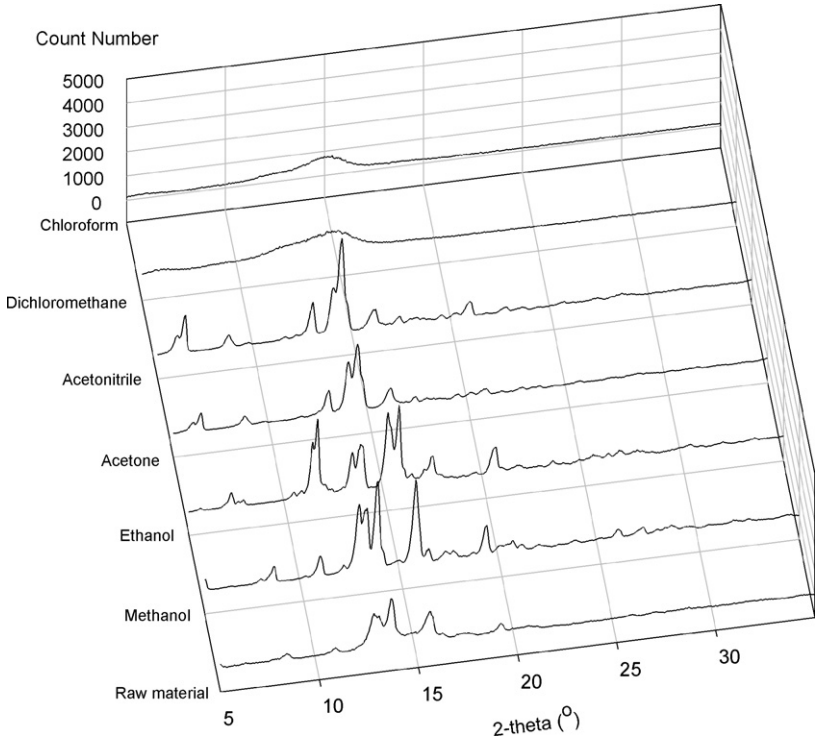

Fig. 4. PXRD patterns of oleanolic acid samples crystallized by fast cooling method under different solvent systems.

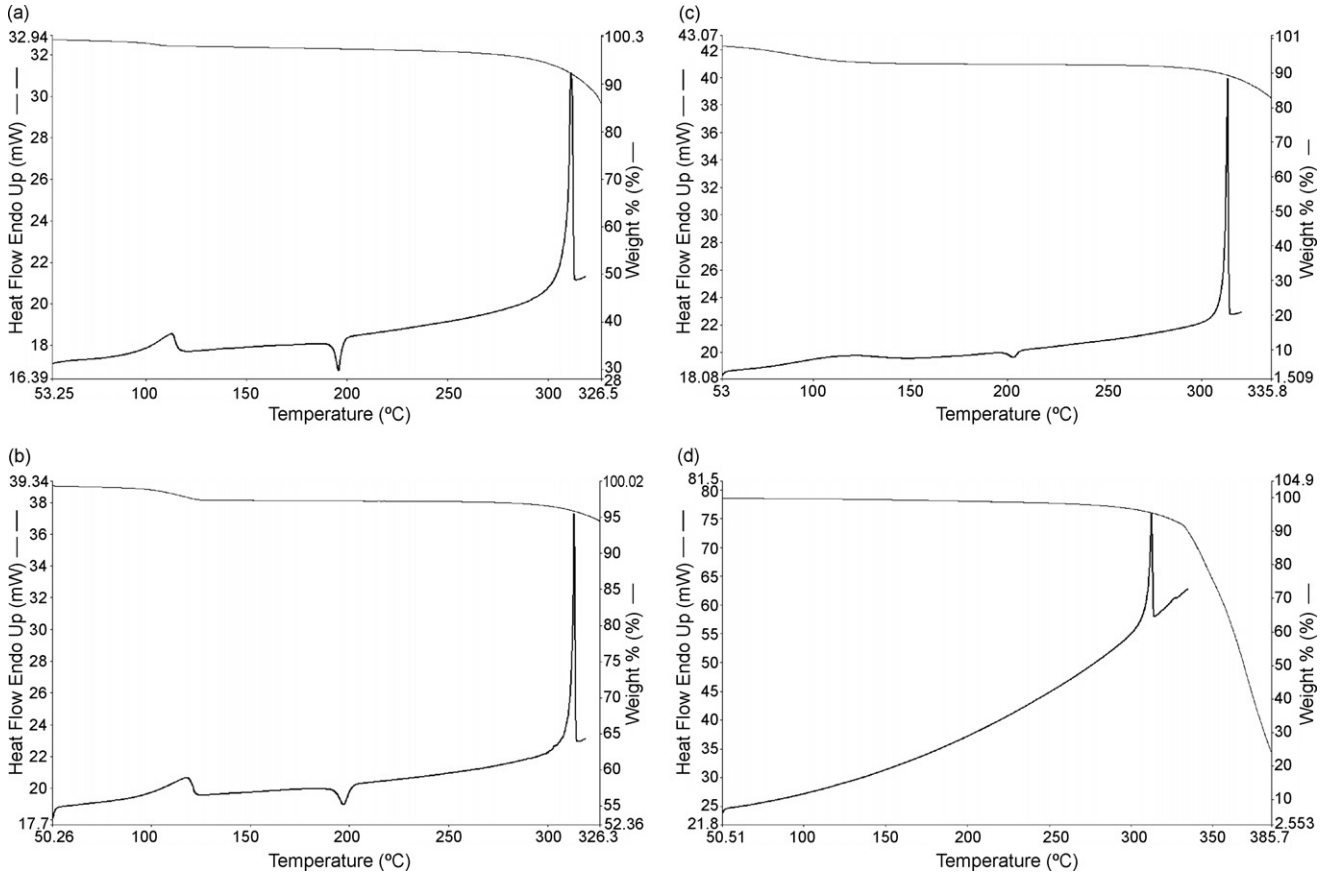

Fig. 5. DSC and TGA curves of (a) oleanolic acid raw material; (b) oleanolic acid methanol solvate; (c) oleanolic acid ethanol solvate; (d) oleanolic acid non-solvate.

and acetone, (OA-methanol, OA-ethanol and OA-acetone) were then subjected to further physicochemical characterization. The DSC and TGA curves of OA–RW and OA-methanol showed similar patterns (Fig. 5a and b). The first endothermic peak was around 100–115 °C (OA–RW: 103.43 °C; OA-methanol: 112.28 °C), with concomitant weight loss of 0.7% (w/w) and 1.1% (w/w) in the TGA for OA–RW and OA-methanol, respectively. The first endothermic peak was followed by an exothermic peak around 190–195 °C (OA–RW: 194.23 °C; OA-methanol: 193.83 °C), and a second, sharp endothermic peak around 310–313 °C (OA–RW: 310.83 °C; OA-methanol: 312.57 °C). No further weight loss was observed after the endothermic peak around 100–115 °C until the second endothermic peak around 310–313 °C (Fig. 5a and b). For OA-ethanol, the first endothermic peak at 73.04 °C was much broader than those of OA–RW and OA-methanol (Fig. 5c). The concomitant loss was 4.7% (w/w). The exothermic peak was at 198.25 °C, and a second, sharp endothermic peak appeared at 312.13 °C (Fig. 5c). For OA-acetone, no thermal event was observed until an endothermic peak at 311.023 °C, and weight loss was observed only after the endothermic transition (Fig. 5d). All these observations suggest that OA-acetone was a non-solvate crystalline form of OA.

VT-PXRD is a valuable tool for evaluating thermal events in crystalline materials. VT-PXRD patterns for OA–RW, OA-methanol, OA-ethanol and OA-acetone are shown in Fig. 6a–d. As the vacuum was applied inside the VT-PXRD sample chamber, temperature shifts appeared compared with the thermal analysis data. In OA–RW, OA-methanol and OA-ethanol, a phase transformation was evident between 30 and 150 °C. All three of these crystalline materials had the same structure as OA-acetone after the exothermic peak around 195 °C (Fig. 6a–d), indicating that recrystallization into the non-solvate form was responsible for the exothermic events evident in the DSC curves (Fig. 5a–c). In addition, the absence of any weight loss during the TGA of OA-acetone (Fig. 5d), together with the fact that the HPLC-determined fraction of oleanolic acid in the OA-acetone was 105.5 ± 3.5% (w/w), further confirmed that OA-acetone must be a non-solvate crystal.

The OA content of the OA-methanol and OA-ethanol were 89.6 ± 3.0% (w/w) and 96.2 ± 3.8% (w/w), respectively, as determined by HPLC. GC revealed that the methanol and ethanol contents of the OA-methanol and OA-ethanol were 4.3% (w/w) and 7.4%, respectively, which is larger than the weight loss evident in the TGA curves. The apparent difference between the TGA and GC results is probably due to the equilibration procedure during the TGA runs, where adsorbed methanol and ethanol may have become desorbed under the continuous flow of dry nitrogen gas at 50 ml min^{-1}. There should, in contrast, have been minimal evaporation during the GC analyses. After air drying for 1 month in a dark chamber at room temperature, the ethanol content of the OA-ethanol had dropped from 7.4 to 0.9%, but its PXRD pattern remained unchanged (data not shown). OA-methanol showed the same behavior.

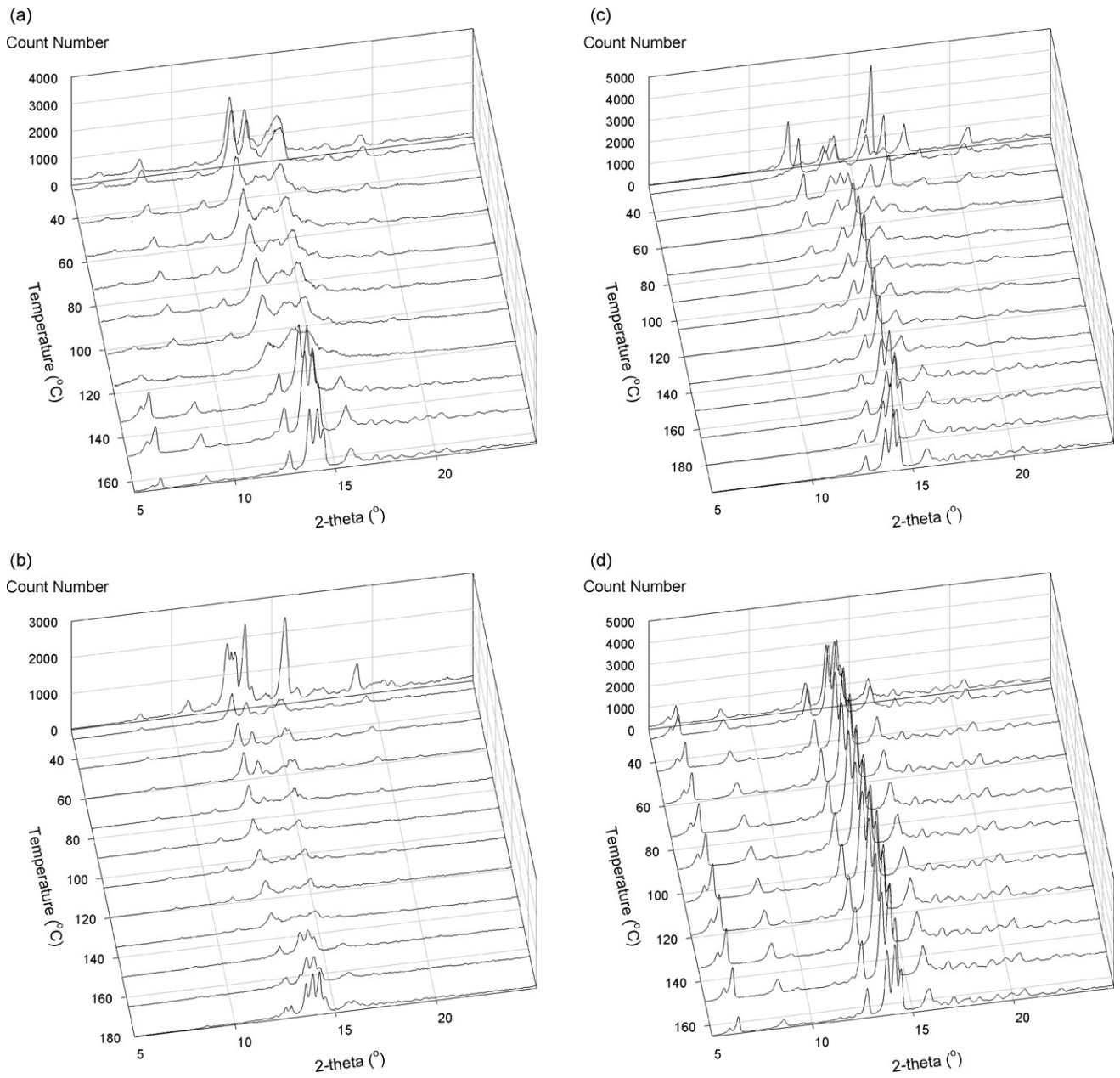

Fig. 6. VT-PXRD patterns for (a) oleanolic acid raw material; (b) oleanolic acid methanol solvate; (c) oleanolic acid ethanol solvate; (d) oleanolic acid non-solvate.

Given their distinctive PXRD patterns, the endothermic peaks around 100–115 °C in the DSC curves, the decrease in weight during TGA analysis, and the data from the HPLC and GC assays, it is evident that OA-methanol and OA-ethanol should be oleanolic solvates, though the stoichiometric ratio could not be readily determined in this study. Both desolvated OA-methanol and OA-ethanol were quite stable at room temperature, but they readily made a solid-state transformation to the same crystalline structure as OA-acetone at elevated temperatures, as evidenced in both the VT-PXRD patterns and the thermal analysis results. Compared with OA-methanol, the desolvation endothermic peak in the DSC curve of OA-ethanol was shallower and broader, suggesting that ethanol was less tightly bound inside the solvate than methanol.

The oleanolic acid content of the OA–RW was 104.6 ± 3.2% (w/w) according to the HPLC results. The methanol content was undetectable by GC. The pharmaceutical grade material may have been prepared through methanol crystallization, followed by special treatment to remove any residual methanol, vacuum drying perhaps. Therefore, OA–RW could in fact be the desolvated oleanolic acid methanol solvate. Careful examination of its PXRD pattern (Fig. 6a) revealed that there were also some amorphous domains in the material.

The FTIR spectra of the OA–RW, OA-methanol, OA-ethanol and OA-acetone at room temperature are shown in Fig. 7a. The differences in the hydroxyl group region between 2800 and 3800 cm^{-1} and carbonyl group region around 1700 cm^{-1} suggest significant differences in inter- and intra- molecular

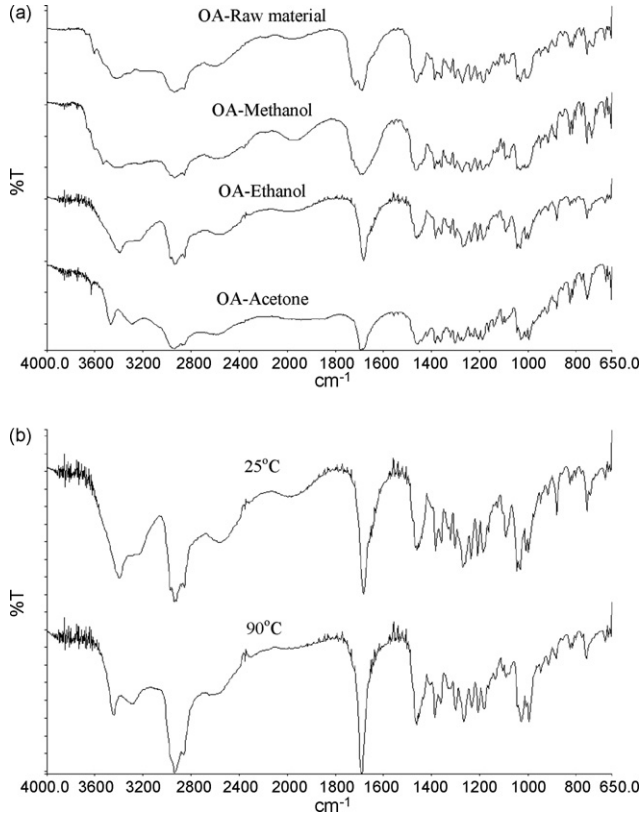

Fig. 7. (a) FTIR spectra of various oleanolic acid samples at 25 °C; (b) FTIR spectra of oleanolic acid ethanol solvate at 25 and 90 °C.

hydrogen bonding networks in the crystal matrix, particularly for the functional groups –OH, C=O and –COOH (Fig. 1a). Residual solvent molecules adsorbed on the crystal surface should have minimal impact on the FTIR spectra, as the FTIR

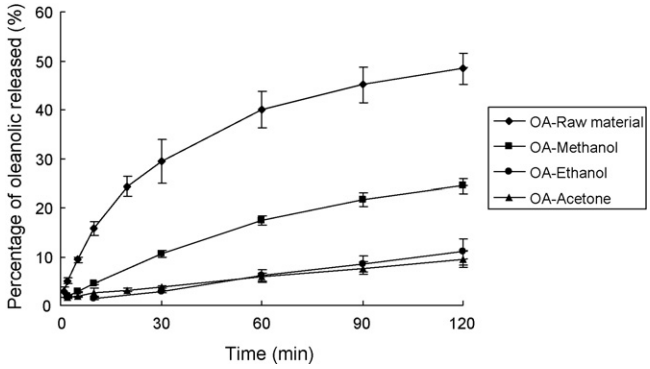

Fig. 8. Powder dissolution study for various oleanolic acid samples.

spectra at 90 °C were similar to those at room temperature, except for OA-ethanol (Fig. 7b). A number of important peak shifts were observed from 25 to 90 °C in OA-ethanol: 3395.5 cm^{-1} → 3448.4 cm^{-1}; 3222.9 cm^{-1} → 3291.4 cm^{-1}; 1681.9 cm^{-1} → 1692.2 cm^{-1}; 1034.1 cm^{-1} → 1027.2 cm^{-1}, corresponding to internal crystal structure rearrangements. If higher temperatures could be reached in VT-FTIR, further peak shifts might be observed.

As mentioned before, the OA–RW did not show any detectable solubility (<1 μg/ml by HPLC) in buffer solutions (at pH 1 and 7) after 120 min at 37 °C. Hence, 1% sodium lauryl sulphate in distilled water was used as the medium for both powder dissolution studies. The powder dissolution profiles are shown in Fig. 8. Both intrinsic and intrinsic dissolution rates of OA–RW were obviously faster than those of the other materials. Its higher specific surface area could be the reason (Table 1). In addition, changes in PXRD patterns are evident in OA–RW after dissolution (Fig. 9). There was a decrease of crystallinity evident in the PXRD patterns of OA–RW after

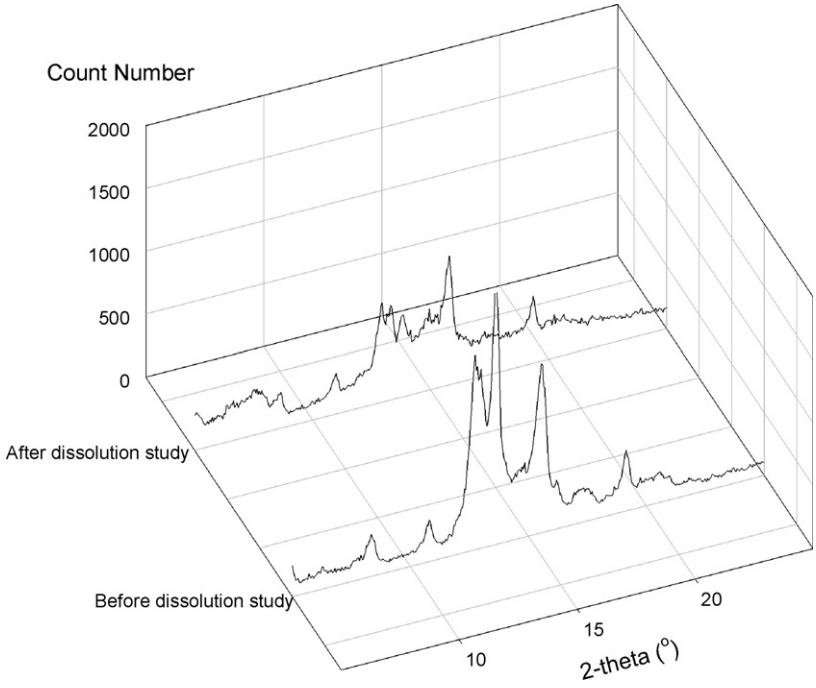

Fig. 9. PXRD patterns of OA-raw material before and after dissolution study.

Table 1
Specific surface area, initial and intrinsic dissolution rates of oleanolic acid samples

Sample	Specific surface area ($m^2\ g^{-1}$)	Initial dissolution rate ($\mu g\ ml^{-1}\ min^{-1}$)	Intrinsic dissolution rate ($\mu g\ min^{-1}\ cm^{-2}$)
OA-raw material	35.47	3.368 (0.317)	0.221 (0.021)
OA-methanol	5.11	0.187 (0.007)	0.088 (0.003)
OA-ethanol	6.78	0.062 (0.015)	0.021 (0.005)
OA-acetone	13.98	0.111 (0.037)	0.019 (0.006)

the solubility study (Fig. 9), explaining the distinctive powder dissolution profile of OA–RW. The observed difference in OA–RW and OA-methanol is probably due to difference in crystallinity in the samples. For the other crystal forms, methanol and ethanol solvates show higher intrinsic dissolution rates than the non-solvated form because of the favorable reduction in free energy through the mixing of methanol/ethanol with water.

4. Conclusions

An oleanolic acid non-solvate, methanol solvate and ethanol solvate have been prepared and characterized. The pharmaceutical grade oleanolic acid raw material is likely to have been a desolvated methanol solvate. Solid-state transitions of both the methanol and ethanol solvates have also been demonstrated.

Acknowledgements

Financial support from the Macao Polytechnic Institute (Project No: RP/ESS-4/2006 for HHYT) and through a Competitive Earmarked Research Grant from the Research Grants Council of the Hong Kong Special Administrative Region (Project No: 610805 for CKC and WHB) is gratefully acknowledged.

References

Chen, J.H., Xia, Z.H., Tan, R.X., 2003. High-performance liquid chromatographic analysis of bioactive triterpenes in *Perilla frutescens*. J. Pharm. Biomed. Anal. 32, 1175–1179.

Chen, Y., Liu, J., Yang, X., Zhao, X., Xu, H., 2005. Oleanolic acid nanosuspensions: preparation, *in-vitro* characterization and enhanced hepatoprotective effect. J. Pharm. Pharmacol. 57, 259–264.

Jeong, D.W., Kim, Y.H., Kim, H.H., Ji, H.Y., Yoo, S.D., Choi, W.R., Lee, S.M., Han, C.K., Lee, H.S., 2007. Dose-linear pharmacokinetics of oleanolic acid after intravenous and oral administration in rats. Biopharm. Drug Dispos. 28, 51–57.

Liu, J., 2005. Oleanolic acid and ursolic acid: research perspectives. J. Ethnopharmacol. 100, 92–94.

Neil, M.J., Smith, A., Heckelman, P.E., 2001. The Merck Index, 13th ed. Merck & Co., Inc., Whitehouse Station, USA.

Song, M., Hang, T., Wang, Y., Jiang, L., Wu, X., Zhang, Z., Shen, J., Zhang, Y., 2006. Determination of oleanolic acid in human plasma and study of its pharmacokinetics in Chinese healthy male volunteers by HPLC tandem mass spectrometry. J. Pharm. Biomed. Anal. 40, 190–196.

Tang, X.H., Gao, J., Fang, F., Chen, J., Xu, L.Z., Zhao, X.N., Xu, Q., 2005. Hepatoprotection of oleanolic acid is related to its inhibition on mitochondrial permeability transition. Am. J. Chin. Med. 33, 627–637.

Wang, D.R., 2003. Recent progress in oleanolic acid research. Tianjin Pharm. 15, 56–58 [article in Chinese].